# OMEGA Cryogenic Target Designs

The achievement of high-density implosions using ignition-relevant pulse shapes and cryogenic targets on OMEGA is an important milestone on the path to attaining direct-drive ignition at the National Ignition Facility (NIF). The OMEGA Cryogenic Target Handling System is undergoing final tests and will soon be commissioned for $D_2$ implosion experiments. Cryogenic targets have also been designed for this system with the primary criterion of being *hydrodynamically equivalent* to the ignition capsule designs. In this context, the constraints placed on OMEGA cryogenic target designs include similar peak shell velocities, hot-spot convergence, in-flight aspect ratio, and stability properties as the NIF designs. NIF designs have been discussed previously in Ref 1. In this article, we report on the cryogenic OMEGA target design and compare its physical behavior with the $\alpha = 3$ ignition NIF design.

The basis for the OMEGA designs is the NIF direct-drive $\alpha = 3$ ignition design, which consists of a 340-$\mu$m DT-ice layer encased in a thin (<3-$\mu$m) plastic capsule of 1.69-mm outer radius. One-dimensional hydrodynamic scaling arguments[2] can then be used to guide the design of OMEGA cryogenic targets. The laser energy ($E$) required to contribute to a given plasma thermal energy scales roughly as the radius of the capsule ($R$) according to $E \sim R^3$. The NIF is designed to provide 1.5 MJ of energy; OMEGA is capable of delivering 30 kJ. Thus, the radius of an OMEGA capsule will be approximately 0.3 times the NIF design (see Fig. 82.1).

Figure 82.2 shows the power history for the NIF and OMEGA pulses. The NIF laser pulse irradiating the ignition design is a 9.25-ns shaped pulse consisting of a 10-TW, 4.25-ns foot rising to a 450-TW pulse for 2.5 ns. The corresponding laser pulse for the OMEGA design is determined by noting that the time ($t$) or duration of the laser pulse scales as the confinement time and is roughly proportional to the radius of the target; therefore[2] $t \sim R$. The scaling of the peak power ($P$) in the laser pulse can be obtained from the energy and time scaling; therefore,[2] $P \sim R^2$. Consequently, the length of the laser pulse shrinks from 9.25 ns in the $\alpha = 3$ ignition target design to 2.5 ns for the OMEGA cryogenic target design. The peak power using $P \sim R^2$ then scales to 32 TW. Processes other than hydrodynamics, such as radiation, thermal transport, and thermonuclear burn, do not scale in a simple manner between the ignition designs and the OMEGA cryogenic designs. We will show, however, that these energy-scaled targets possess similar 1-D behavior and instability growth as the ignition designs, thus meeting the requirement of hydrodynamic equivalence.

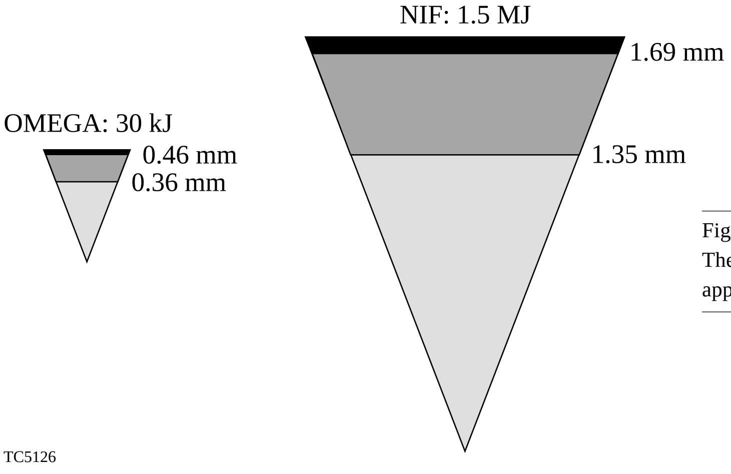

Figure 82.1
The NIF and OMEGA capsule designs. The radius of the OMEGA design is approximately 0.3 times that of the NIF design.

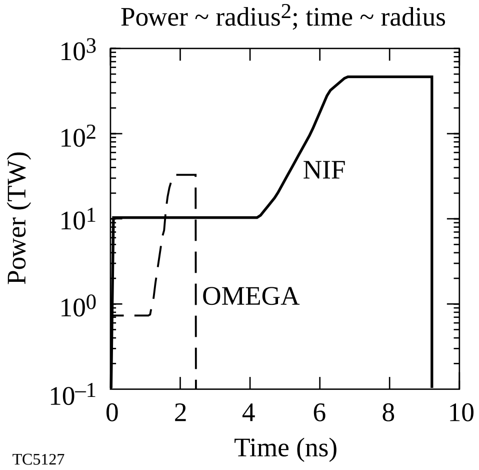

Figure 82.2
The NIF and OMEGA pulse shapes.

The timing of *two* shocks is critical to determining the overall performance of the direct-drive ignition target design. The two distinct shocks in this design are launched into the target at the start of the laser pulse and during its rise to the main drive intensity. The position of the shocks in the target can be calculated from the radial logarithmic derivative of the pressure. Figure 82.3 is a contour map of this quantity [$d(\ln P)/dr$] as a function of the Lagrangian coordinate and time for the ignition and the OMEGA design. Time has been normalized to the incident laser energy, with $t = 1.0$ corresponding to the end of the laser pulse. This normalization will allow us to compare the two designs at the same stage of the implosion. The darker, more-intense regions represent a larger gradient in pressure and thus capture the position of the shocks. The OMEGA design shows similar shock-timing behavior as that of the ignition design for the first shock. The second shock, however, arrives slightly later in the OMEGA design than in the ignition design in normalized time units. This is a consequence of lower laser-energy absorption in the OMEGA design. Absorption in direct-drive designs is primarily via inverse bremsstrahlung, which depends on the density scale length. The NIF designs typically have scale lengths that are 2 to 3 times longer than OMEGA, which leads to an absorption fraction for the ignition design of 60% on the NIF and 40% on OMEGA.

At the time the first shock breaks out of the rear of the ice surface, a rarefaction wave travels back through the ice layer in the outward direction. This rarefaction wave results in a decreasing density gradient in the inward radial direction. The second shock, which is caused by the rise of the main pulse, then travels through this decreasing density gradient. This serves to increase the adiabat ($\alpha$) of the ice layer. Since the second shock in the OMEGA design arrives later (in normalized time units) than in the NIF design, the rear ice surface decompresses more than in the ignition design. Consequently, the OMEGA design has a slightly higher adiabat ($\alpha = 3.2$) than the ignition design ($\alpha = 3$).

The adiabat of the implosion is defined as the ratio of the pressure of the cold fuel to the Fermi degenerate pressure and is an important figure of merit for the overall performance of target designs. Lower adiabat implosions have higher one-dimensional performance since less laser energy is needed to

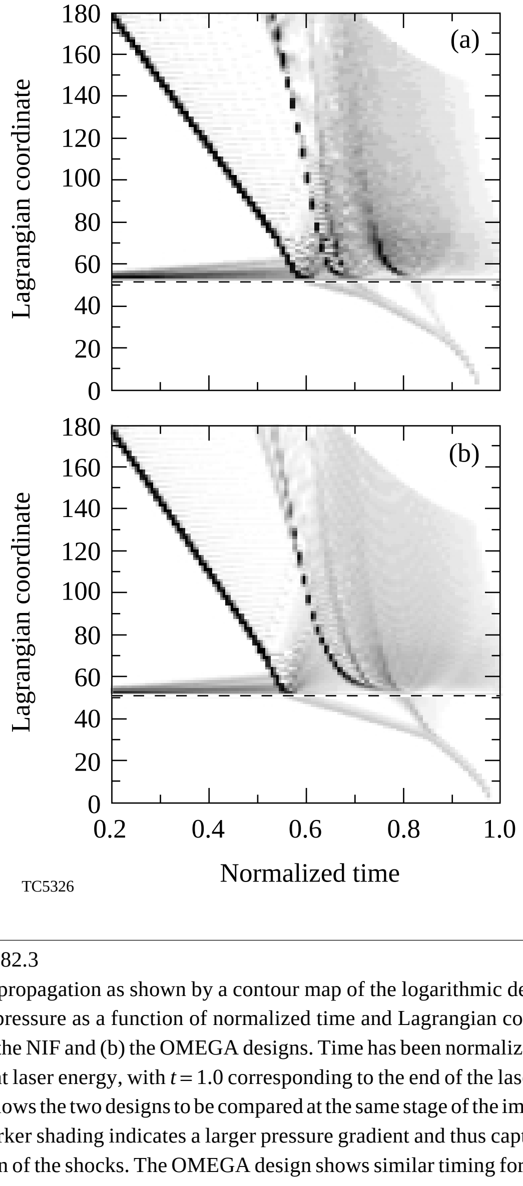

Figure 82.3
Shock propagation as shown by a contour map of the logarithmic derivative of the pressure as a function of normalized time and Lagrangian coordinate for (a) the NIF and (b) the OMEGA designs. Time has been normalized to the incident laser energy, with $t = 1.0$ corresponding to the end of the laser pulse. This allows the two designs to be compared at the same stage of the implosion. The darker shading indicates a larger pressure gradient and thus captures the position of the shocks. The OMEGA design shows similar timing for the first shock but a delayed second shock compared to the NIF design.

compress a cold fuel than a warm fuel. The ablation velocity, however, depends directly on the adiabat (~$\alpha^{3/5}$); thus, the Rayleigh–Taylor (RT) growth rates decrease with the adiabat. Higher adiabat implosions, therefore, are more stable to the acceleration-phase RT instability. To ensure similar performance between the NIF and OMEGA cryogenic capsules, the cold fuel layer should have similar adiabats. Plotting the pressure-density trajectory of the Lagrangian cells used in the simulation will show the adiabatic history of target designs. Figure 82.4 is such a plot for both the NIF design and the OMEGA design; also shown is the $\alpha = 3$ adiabat line (dashed). The NIF design obviously accesses a larger portion of phase space than the OMEGA design. Only the extremely compressed and high-density region is inaccessible by the OMEGA design. Table 82.I, which lists other key one-dimensional parameters, indicates that the OMEGA and NIF designs have similar peak shell velocities, hot-spot convergence ratios, and in-flight aspect ratios. To compare an igniting and non-igniting target, we have defined the hot spot as the ratio of the initial outer radius to the radius that contains 90% of the yield at the time of peak neutron production when propagating burn has been switched off.

Implosion efficiency can be quantified in two ways: The *hydrodynamic efficiency* is defined as the ratio of the kinetic energy of the imploding target to the absorbed energy. The *coupling efficiency* is defined as the ratio of the kinetic energy of the imploding target to the incident energy. Although OMEGA has a similar hydrodynamic efficiency to the NIF, the reduced absorption fraction leads to a lower coupling efficiency.

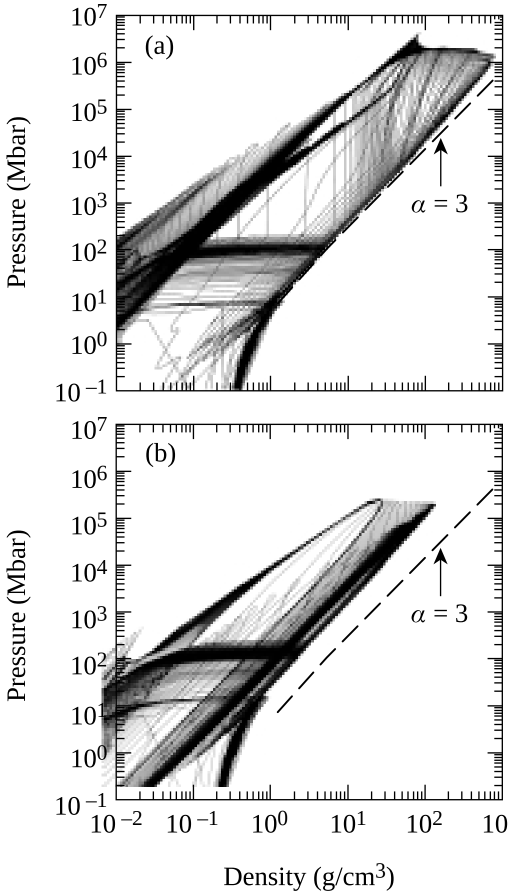

Figure 82.4
The density-pressure trajectories for each Lagrangian cell used in the simulations of (a) NIF and (b) OMEGA designs. Also shown (dashed line) is the $\alpha = 3$ adiabat line.

Table 82.I: Comparison of one-dimensional parameters between the NIF and OMEGA cryogenic target designs.

| | NIF | OMEGA |
|---|---|---|
| Absorption fraction | 60% | 40% |
| Hydrodynamic efficiency | 11.0% | 11.5% |
| Coupling efficiency | 7% | 4.5% |
| Peak shell velocity (cm/s) | $4.0 \times 10^7$ | $3.7 \times 10^7$ |
| Hot-spot convergence ratio | 28 | 20 |
| In-flight aspect ratio | 60 | 50 |
| Peak areal density (mg/cm$^2$) | 1200 | 300 |
| Neutron-averaged ion temperature (keV) | 30 | 4 |
| Neutron yield | $2.5 \times 10^{19}$ | $1.8 \times 10^{14}$ |

The NIF design is expected to have different plasma physics issues compared to the OMEGA design. The density and velocity scale lengths at the tenth- and quarter-critical surfaces primarily determine the intensity threshold for plasma instabilities such as stimulated Raman scattering (SRS), stimulated Brillouin scattering (SBS), and two-plasmon decay (TPD). These instabilities in the ablating plasma can significantly influence laser absorption, the occurrence of hot electrons, and therefore the performance of the target. By comparing the actual intensity to the plasma instability thresholds, the susceptibility of the designs to plasma instabilities can be assessed. The quarter- and tenth-critical surfaces have similar intensities in both cases, which is not surprising since the laser power was scaled with the square of the radius of the pellet; the peak intensity as a result of overlapped beams at the quarter-critical surface is $1.0 \times 10^{15}$ W/cm$^2$ and $6.0 \times 10^{14}$ W/cm$^2$ at the tenth-critical surface for both designs. For the NIF the total overlapped intensity is well above the SBS threshold after about 6 ns; while the single-cluster intensity is comparable to the threshold. The intensity is always below the SRS threshold. As mentioned, OMEGA has shorter scale lengths than the NIF designs. During the rise to the peak of the laser pulse the scale length at the tenth-critical surface in the NIF design rapidly increases to approximately 800 $\mu$m$^{-1}$ and is typically three times larger than the OMEGA design. Therefore, we would expect the OMEGA design to be less susceptible to SRS and SBS than the NIF design. However, both designs are well above threshold for the TPD instability. The NIF design also has a larger volume than OMEGA for the nonlinearly saturated state of the TPD instability to generate hot electrons. Separate experiments have been conducted at LLE to study these plasma physics issues. In these experiments, NIF-scale-length plasmas have been generated using a laser pulse similar in intensity to the NIF pulse. Results to date[3] of the high-intensity drive portion of the NIF pulse show little evidence of SRS, suggesting that this instability will have an insignificant effect on the performance of the ignition design.

Hydrodynamic instabilities are the second source of deviations from one-dimensional hydrodynamic simulations. The RT instability can degrade target performance by breaking the spherical symmetry of the implosion. The RT instability occurs twice during the implosion: at the outer ablation surface as the shell accelerates inward and at the hot spot–main fuel layer interface as the capsule decelerates at the end of the implosion. Four sources of nonuniformity primarily seed the RT instability: (1) laser imprinting, (2) outside capsule finish, (3) drive asymmetry, and (4) inner-DT-ice roughness. An important component of the OMEGA campaign will be to experimentally determine the maximum allowable levels of these sources of nonuniformities for the NIF laser and direct-drive ignition targets. OMEGA cryogenic targets must, therefore, have similar stability properties to the NIF designs to ensure that the extrapolation of these results to NIF targets will be valid.

Imprint levels are expected to be smaller on OMEGA than on the NIF. The level of laser imprint in both the NIF and OMEGA direct-drive targets can be quantified in terms of the imprint efficiency, which is defined as the ratio of the amplitude of the ablation surface nonuniformity to the percent of laser nonuniformity. We determine this quantity using two-dimensional (2-D) *ORCHID* simulations, each with a single-mode laser nonuniformity, for NIF and OMEGA designs. These *ORCHID* simulations included the following laser-smoothing techniques: (1) a phase-plate spectrum appropriate to the spot size, (2) a polarization-smoothing wedge, and (3) 2-D smoothing by spectral dispersion (SSD) at two UV bandwidths (0.5 THz$_{\text{UV}}$ and 1 THz$_{\text{UV}}$). We find good agreement between the imprint efficiency calculated from *ORCHID* and that obtained from the analytic theory of Goncharov.[4] Using this analytic theory and *ORCHID* simulations, the mode spectrum due to imprint for the NIF and OMEGA designs at the start of the acceleration phase is shown in Fig. 82.5. In the NIF design, the laser has imprinted a surface nonuniformity equal to $\sigma_{\text{rms}} = 480$ Å (in modes $\ell < 1000$). OMEGA has a corresponding imprinted nonuniformity of $\sigma_{\text{rms}} = 290$ Å. The cusps observed in the mode spectrum are a consequence of dynamic overpressure[4] that causes the imprinted mode to oscillate with a period proportional to the wavelength of the mode. The acceleration phase begins when the rarefaction wave from the rear surface reaches the ablation surface; therefore, the time

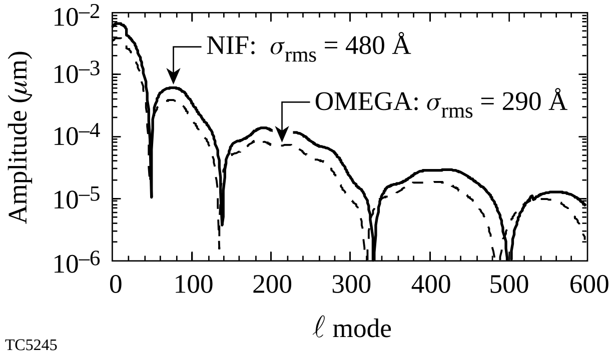

Figure 82.5
Modal spectrum of the surface amplitude due to imprint from a 1-THz$_{\text{UV}}$ 2-D SSD smoothed laser for the NIF and OMEGA designs at the start of the acceleration phase.

when this phase begins is roughly proportional to the shell thickness. The cusps in the imprint spectrum will consequently occur for wavelengths that are at a minimum when the acceleration phase begins. For the NIF design, the period of oscillation is three times that of the OMEGA design; however, the acceleration phase begins approximately three times later than the OMEGA design, so the cusps occur at the same part of the $\ell$-mode spectrum for both designs. Scaling arguments can be invoked to determine the relation between imprint levels on OMEGA and NIF targets. Since the laser energy deposited at the critical surface is thermally conducted to the ablation surface, significant reductions in the level of imprint-induced nonuniformities can be obtained by thermal smoothing over this *stand-off* distance. Dimensional considerations suggest that imprint levels should vary as $kD_c$ (where $k$ is the perturbation wave number and $D_c$ is the distance between the energy absorption region and the ablation surface). Imprint essentially ends when the laser decouples from the target, i.e., when $kD_c \sim 1$; therefore, a longer wavelength should imprint less than a shorter wavelength. A given $\ell$ mode on OMEGA has a wavelength that is approximately one-third of the same $\ell$ mode on the NIF direct-drive target. Thus a single beam on OMEGA will imprint one-third as much as on the NIF for the same $\ell$ mode. However, since NIF has approximately four times the number of overlapped beams, imprint for OMEGA design will be two-thirds that of the NIF design.

Next, we study the evolution of the shell during the acceleration phase of the implosion. The OMEGA designs have an overdense shell thickness that is approximately one-third the NIF-shell thickness, where the shell thickness is defined as the distance between the $1/e$ points of the maximum density. If the two designs have the same initial seed and RT $e$-foldings during the acceleration phase, the OMEGA design's mix-width region will be a greater percentage of the overdense shell. Figure 82.6 shows the results of an instability post-processor to 1-D hydrocode *LILAC* simulations. This post-processor uses a self-consistent model[5] to study the evolution of perturbations at the ablation front and the back surface of an accelerated spherical shell. The model includes the ablative Richtmyer–Meshkov (RM),[6] RT, and Bell–Plesset (BP) instabilities, and 3-D Haan saturation.[7] The model consists of two differential equations (describing the ablation- and inner-surface perturbations) obtained by solving the linearized conservation equations in the DT gas, the shell, and the blowoff plasma regions. The seeds for the nonuniformity processor were (1) the imprint caused by 1-THz$_{\mathrm{UV}}$, 2-D SSD; (2) an outer capsule roughness of 840 Å (in an $\ell$-mode spectrum taken from Weber[8]); and (3) an inner-ice-surface roughness of 2 $\mu$m [with a spectrum of the form $\sigma \sim \ell^{-1.5}$ (Ref. 9)]. Figure 82.6 shows the overdense shell thickness and the mix width for the NIF and OMEGA designs. Both designs survive the acceleration phase, i.e., the mix width is less than the shell width; however, the NIF mix width is approximately 30% of the overdense shell, whereas the OMEGA design's mix width is almost 90% of the shell thickness. Thus the OMEGA design has a lower safety factor for survival through the acceleration phase than the $\alpha = 3$ NIF design for a given level of laser and target nonuniformity.

During the implosion the outer-surface perturbation *feeds through* to the inner surface, which can then grow via the RT instability during the deceleration phase. The feedthrough for a given $\ell$ mode scales approximately as $kD_o$, where $D_o$ is the overdense shell thickness. Since the increase in shell thickness for the NIF target is compensated for by the smaller wavelength for the same $\ell$ mode, the NIF and OMEGA designs are predicted to have similar amounts of feedthrough. Figure 82.7 shows the mode spectrum at the inner surface of the DT ice for both designs at the onset of the deceleration phase. The mode spectrum is heavily weighted toward the low $\ell$ mode of the spectrum, with most of the power contained below $\ell \sim 20$. The higher level of imprint in the NIF design compared to OMEGA

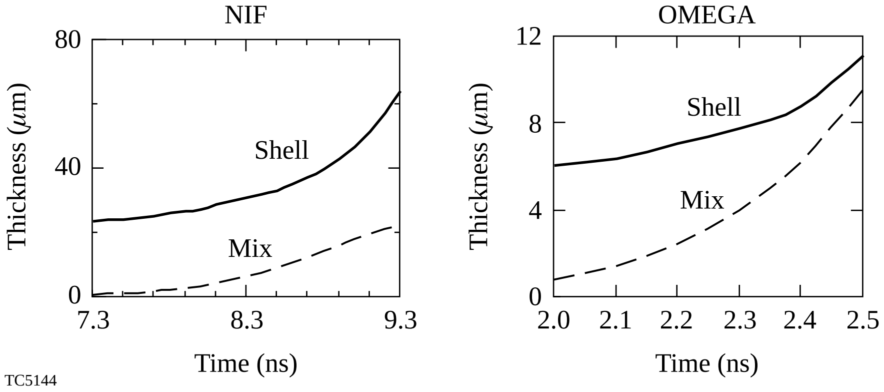

Figure 82.6
The overdense shell thickness and mix width for the NIF design and the OMEGA design during the acceleration phase. In both cases the overdense shell thickness is larger than the mix width, which implies that both designs will survive the acceleration phase.

has led to a higher amount of feedthrough in the range at which imprint dominates ($10 < \ell < 100$). For low $\ell$ modes ($\ell < 10$), where the effect of the inner ice surface is dominant, the mode amplitudes are comparable in both cases. The instability postprocessor cannot self-consistently determine the degradation in target yield for a given initial nonuniformity level. We therefore use a limited number of *ORCHID* simulations to determine the effect of these levels of inner-ice distortions at the start of the deceleration phase (predicted by the instability postprocessor) on the overall target performance.

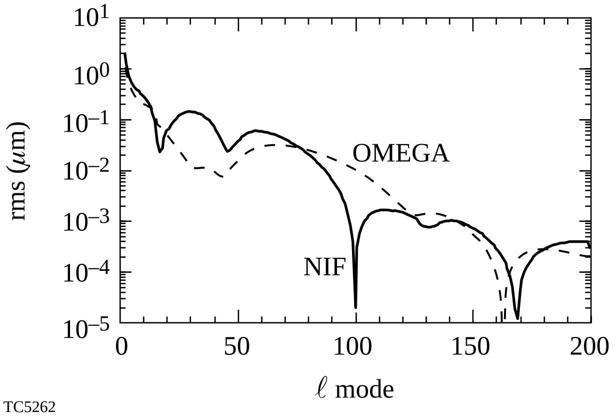

Figure 82.7
The mode spectrum of the NIF (solid line) and OMEGA (dashed line) designs at the onset of the deceleration phase.

The *ORCHID* simulations are initialized at the start of the laser pulse with perturbations on the rear inner ice surface only (the outer surface and laser are assumed to be perfect). As we have seen above, most of the power on the rear surface at the onset of deceleration is concentrated in the low-$\ell$-mode part of the spectrum, so the *ORCHID* calculations contain only modes up to $\ell = 50$ (in contrast, the postprocessor calculations take into account modes up to $\ell = 1000$). Various initial spectra of the form $\sigma \sim \ell^{-\beta}$ were simulated to take into account the four seed terms.[9] The *ORCHID* calculations simulate the implosion through peak compression and burn. The spectra at the start of the deceleration phase obtained from the *ORCHID* simulations are compared to the spectra obtained from the instability postprocessor. This comparison is used to relate the postprocessor analysis to the full 2-D *ORCHID* simulations and obtain the yield for a given level of laser and target nonuniformity. It has been shown previously[9] that the $\alpha = 3$ NIF target gain can be written as a function of $\bar{\sigma}$, where

$$\bar{\sigma}^2 = 0.06\,\sigma^2_{\ell<10} + \sigma^2_{\ell\geq 10};$$

$\sigma^2_{\ell<10}$ and $\sigma^2_{\ell\geq 10}$ are the rms nonuniformity of modes below and above 10, respectively. The instability postprocessor gives $\bar{\sigma}$ at the onset of the deceleration phase for different initial conditions (laser imprint and surface roughness.) By comparing the amplitude and mode spectrum it is possible to relate the reduction in target performance for a given initial nonuniformity. For the $\alpha = 3$ NIF design the instability analysis with an initial 1 $\mu$m of inner ice nonuniformity, 840-Å outer surface roughness, and 1-THz$_{\text{UV}}$, 2-D SSD illumination, the resulting $\bar{\sigma}$ is 1.3 $\mu$m. As we have already seen, the OMEGA design imprints less that the NIF design. Power balance and inner-ice-surface roughness are likely to be similar for both laser configurations. We use the same characterization of the nonuniformity in the deceleration phase for the non-igniting OMEGA target to obtain the neutron yield as a function of $\bar{\sigma}$. For the OMEGA design the instability analysis with the same initial conditions as the NIF capsule leads to a $\bar{\sigma}$ of 0.9 $\mu$m. Figure 82.8 shows the normalized (to 1-D) yield as a function of the deceleration nonuniformity parameter $\bar{\sigma}$. The OMEGA design has a larger reduction in yield for a given level of $\bar{\sigma}$ than the NIF design. This can be attributed to the OMEGA design's smaller hot-spot radius compared to that of the NIF design, which makes the OMEGA hot spot more easily disrupted by the penetration of cold spikes from the main fuel layer. For the same initial conditions, however, the value of $\bar{\sigma}$ is different between the

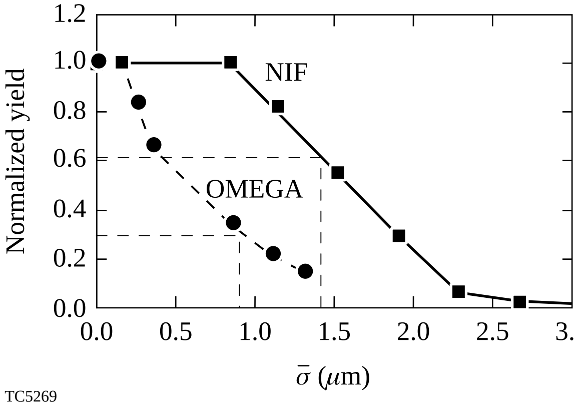

Figure 82.8
The yield, normalized to the 1-D result, as a function of $\bar{\sigma}$, the total nonuniformity at the start of the deceleration phase.

two designs. For the case outlined above, the NIF has a $\bar{\sigma}$ of 1.3 $\mu$m, which leads to a reduction to 60% of 1-D yield (giving a gain of 28), whereas the OMEGA design has a $\bar{\sigma}$ of 0.9 $\mu$m for the same conditions, which leads to a yield of 30% of 1-D.

This article has described the current target designs for the soon-to-be-commissioned OMEGA Cryogenic Target Handling System. These designs are energy scaled from the direct-drive ignition designs for the NIF with a major goal of experimentally studying the various sources of nonuniformity and their influence on target performance. The OMEGA and the NIF designs have been shown to have similar 1-D behavior and stability properties, which will facilitate the extrapolation of the cryogenic target studies on OMEGA to NIF targets. The smaller hot spot in the OMEGA design implies, however, that OMEGA cryogenic targets will be more sensitive to instability growth than the NIF direct-drive ignition targets. Our stability analyses are consistent with this observation and predict that with 1-THz$_{\mathrm{UV}}$, 2-D SSD, and 1 $\mu$m of inner-ice-surface roughness we should obtain approximately 30% of the 1-D yield from the OMEGA cryogenic targets. Using the same analysis tools and similar target and laser uniformity levels, we predict that the $\alpha = 3$ direct-drive ignition design will give a gain of 28 on the NIF, a reduction to 60% of the 1-D yield.

## ACKNOWLEDGMENT

This work was supported by the U.S. Department of Energy Office of Inertial Confinement Fusion under Cooperative Agreement No. DE-FC03-92SF19460, the University of Rochester, and the New York State Energy Research and Development Authority. The support of DOE does not constitute an endorsement by DOE of the views expressed in this article.

## REFERENCES

1. Laboratory for Laser Energetics LLE Review **79**, 121, NTIS document No. DOE/SF/19460-317 (1999). Copies may be obtained from the National Technical Information Service, Springfield, VA 22161.
2. K. A. Brueckner and S. Jorna, Rev. Mod. Phys. **46**, 325 (1974).
3. S. P. Regan, D. K. Bradley, A. V. Chirokikh, R. S. Craxton, D. D. Meyerhofer, W. Seka, R. W. Short, A. Simon, R. P. J. Town, B. Yaakobi, J. J. Caroll III, and R. P. Drake, Phys. Plasmas **6**, 2072 (1999).
4. V. N. Goncharov, S. Skupsky, T. R. Boehly, J. P. Knauer, P. McKenty, V. A. Smalyuk, R. P. J. Town, O. V. Gotchev, R. Betti, and D. D. Meyerhofer, Phys. Plasmas **7**, 2062 (2000).
5. V. N. Goncharov, “Self-Consistent Stability Analysis of Ablation Fronts in Inertial Confinement Fusion,” Ph.D thesis, University of Rochester, 1998.
6. V. N. Goncharov, Phys. Rev. Lett. **82**, 2091 (1999).
7. S. W. Haan, Phys. Rev. A **39**, 5812 (1989).
8. S. V. Weber, S. G. Glendinning, D. H. Kalantar, M. H. Key, B. A. Remington, J. E. Rothenberg, E. Wolfrum, C. P. Verdon, and J. P. Knauer, Phys. Plasmas **4**, 1978 (1997).
9. V. N. Goncharov, S. Skupsky, P. W. McKenty, J. A. Delettrez, R. P. J. Town, and C. Cherfils-Clerouin, “Stability Analysis of Directly Driven OMEGA and NIF Capsules,” to be published in the *Proceedings of the 1999 Inertial Fusion Sciences and Applications Conference*, Bordeaux, France, 12–17 September 1999; also Laboratory for Laser Energetics LLE Review **81**, 1, NTIS document No. DOE/SF/19460-335 (1999). Copies of the LLE Review may be obtained from the National Technical Information Service, Springfield, VA 22161.